Overview of PHENIX Results from the First RHIC Run

W.A. Zajc,[8] for the PHENIX Collaboration:

K. Adcox,[40] S.S. Adler,[3] N.N. Ajitanand,[27] Y. Akiba,[14] J. Alexander,[27] W. Allen,[29] G. Alley,[29] L. Aphecetche,[34] Y. Arai,[14] J.B. Archuleta,[19] J.R. Archuleta,[19] V. Armijo,[19] S.H. Aronson,[3] I. Atatekin,[21] D. Autrey,[18] R. Averbeck,[28] T.C. Awes,[29] K.N. Barish,[5] P.D. Barnes,[19] J. Barrette,[21] B. Bassalleck,[25] S. Bathe,[22] V. Baublis,[30] A. Bazilevsky,[12,32] J. Behrendt,[25] S. Belikov,[12,13] F.G. Bellaiche,[29] S.T. Belyaev,[16] M.J. Bennett,[19] Y. Berdnikov,[35] D.D. Bluhm,[13] M. Bobrek,[29] J.G. Boissevain,[19] S. Boose,[3] S. Botelho,[33] J. Branning,[29] C.L. Britton Jr.,[29] M.L. Brooks,[19] D.S. Brown,[26] N. Bruner,[25] W.L. Bryan,[29] D. Bucher,[22] H. Buesching,[22] V. Bumazhnov,[12] G. Bunce,[3,32] J. Burward-Hoy,[28] S. Butsyk,[28,30] M.M. Cafferty,[19] T.A. Carey,[19] P. Chand,[2] J. Chang,[5] W.C. Chang,[1] R.B. Chappell,[9] L.L. Chavez,[25] S. Chernichenko,[12] C.Y. Chi,[8] J. Chiba,[14] M. Chiu,[8] R.K. Choudhury,[2] T. Christ,[28] T. Chujo,[3,39] M.S. Chung,[15,19] P. Chung,[27] V. Cianciolo,[29] B.A. Cole,[8] D.W. Crook,[9] H. Cunitz,[8] D.G. D'Enterria,[34] S.Q. Daniel,[29] G. David,[3] H. Delagrange,[34] A. Denisov,[12] A. Deshpande,[32] E.J. Desmond,[3] O. Dietzsch,[33] B.V. Dinesh,[2] A. Drees,[28] A. Durum,[12] D. Dutta,[2] K. Ebisu,[24] M.A. Echave,[19] Y.V. Efremenko,[29] K. El Chenawi,[40] M.S. Emery,[29] H. En'yo,[17,31] M.N. Ericson,[29] S. Esumi,[39] V. Evseev,[30] L. Ewell,[3] T. Ferdousi,[5] D.E. Fields,[25] S.L. Fokin,[16] Z. Fraenkel,[42] S.S. Frank,[29] A. Franz,[3] A.D. Frawley,[9] J. Fried,[3] S.-Y. Fung,[5] J. Gannon,[3] S. Garpman,[20] T.F. Gee,[29] T.K. Ghosh,[40] P. Giannotti,[3] Y. Gil,[42] A. Glenn,[36] A.L. Godoi,[33] Y. Goto,[32] S.V. Greene,[40] M. Grosse Perdekamp,[32] S.K. Gupta,[2] W. Guryn,[3] H.-Å. Gustafsson,[20] J.S. Haggerty,[3] S.F. Hahn,[19] H. Hamagaki,[7] A.G. Hansen,[19] H. Hara,[24] J. Harder,[3] G.W. Hart,[19] E.P. Hartouni,[18] R. Hayano,[38] N. Hayashi,[31] X. He,[10] N. Heine,[22] F. Heistermann,[3] T.K. Hemmick,[28] J. Heuser,[28] M. Hibino,[41] J.S. Hicks,[29] J.C. Hill,[13] D.S. Ho,[43] K. Homma,[11] B. Hong,[15] A. Hoover,[26] J.R. Hutchins,[9] R. Hutter,[28] T. Ichihara,[31,32] K. Imai,[17,31] M.S. Ippolitov,[16] M. Ishihara,[31,32] B.V. Jacak,[28,32] U. Jagadish,[29] W.Y. Jang,[15] J. Jia,[28] B.M. Johnson,[3] S.C. Johnson,[18,28] J.P. Jones Jr.,[29] K.S. Joo,[23] S. Kahn,[3] S. Kametani,[41] Y.A. Kamyshkov,[29] A. Kandasamy,[3] J.H. Kang,[43] M. Kann,[30] S.S. Kapoor,[2] K.V. Karadjev,[16] S. Kato,[39] M.A. Kelley,[3] S. Kelly,[8] M. Kennedy,[9] B. Khachaturov,[42] A. Khanzadeev,[30] A. Khomoutnikov,[35] J. Kikuchi,[41] D.J. Kim,[43] H.J. Kim,[43] S.Y. Kim,[43] Y.G. Kim,[43] W.W. Kinnison,[19] E. Kistenev,[3] A. Kiyomichi,[39] C. Klein-Boesing,[22] S. Klinksiek,[25] L. Kochenda,[30] D. Kochetkov,[5] V. Kochetkov,[12] D. Koehler,[25] T. Kohama,[11] B. Komkov,[30] A. Kozlov,[42] V. Kozlov,[30] P. Kravtsov,[30] P.J. Kroon,[3] V. Kuriatkov,[30] K. Kurita,[31,32] M.J. Kweon,[15] Y. Kwon,[43] G.S. Kyle,[26] R. Lacey,[27] J.G. Lajoie,[13] J. Lauret,[27] A. Lebedev,[13] V.A. Lebedev,[16] D.M. Lee,[19] M.J. Leitch,[19] X.H. Li,[5] Z. Li,[6,31] D.J. Lim,[43] R. Lind,[29] M.X. Liu,[19] X. Liu,[6] Z. Liu,[6] C.F. Maguire,[40] J. Mahon,[3] Y.I. Makdisi,[3] V.I. Manko,[16] Y. Mao,[6,31] L.J. Marek,[19] S.K. Mark,[21] S. Markacs,[8] D. Markushin,[30] G. Martinez,[34] M.D. Marx,[28] A. Masaike,[17] F. Matathias,[28] T. Matsumoto,[7,41] W. McGahern,[3] P.L. McGaughey,[19] D.E. McMillan,[29] E. Melnikov,[12] M. Merschmeyer,[22] F. Messer,[28] M. Messer,[3] Y. Miake,[39] N. Miftakhov,[30] T.E. Miller,[40] A. Milov,[42] S. Mioduszewski,[3,36] R.E. Mischke,[19] G.C. Mishra,[10] J.T. Mitchell,[3] A.K. Mohanty,[2] B.C. Montoya,[19] J.A. Moore,[29] D.P. Morrison,[3] C.G. Moscone,[29] J.M. Moss,[19] F. Mühlbacher,[28] M. Muniruzzaman,[5] J. Murata,[31] S. Nagamiya,[14] Y. Nagasaka,[24] J.L. Nagle,[8] Y. Nakada,[17] B.K. Nandi,[5] J. Newby,[36] L. Nikkinen,[21] S.A. Nikolaev,[16] P. Nilsson,[20] S. Nishimura,[7] A.S. Nyanin,[16] J. Nystrand,[20] E. O'Brien,[3] C.A. Ogilvie,[13] H. Ohnishi,[3,11] I.D. Ojha,[4,40] M. Ono,[39] V. Onuchin,[12] A. Oskarsson,[20] L. Österman,[20] I. Otterlund,[20] K. Oyama,[7,38] L. Paffrath,[3,*] A.P.T. Palounek,[19] C. Pancake,[28] V.S. Pantuev,[28] V. Papavassiliou,[26] B. Pasmantirer,[42] S.F. Pate,[26] C. Pearson,[3] T. Peitzmann,[22] A.N. Petridis,[13] C. Pinkenburg,[3,27] R.P. Pisani,[3] P. Pitukhin,[12] F. Plasil,[29] M. Pollack,[28,36] K. Pope,[36] R. Prigl,[3] M.L. Purschke,[3] S. Rankowitz,[3] I. Ravinovich,[42] K.F. Read,[29,36] K. Reygers,[22] V. Riabov,[30,35] Y. Riabov,[30] G. Richardson,[19] S.H. Robinson,[19] M. Rosati,[13] E. Roschin,[30] A.A. Rose,[40]

R. Ruggiero,[3] S. S. Ryu,[43] N. Saito,[31,32] A. Sakaguchi,[11] T. Sakaguchi,[7,41] H. Sako,[39] T. Sakuma,[31,37] V. Samsonov,[30] T. C. Sangster,[18] R. Santo,[22] H. D. Sato,[17,31] S. Sato,[39] S. Sawada,[14] B. R. Schlei,[19] Y. Schutz,[34] V. Semenov,[12] R. Seto,[5] T. K. Shea,[3] I. Shein,[12] T.-A. Shibata,[31,37] K. Shigaki,[14] T. Shiina,[19] Y. H. Shin,[43] I. G. Sibiriak,[16] D. Silvermyr,[20] K. S. Sim,[15] J. Simon-Gillo,[19] C. P. Singh,[4] V. Singh,[4] F. W. Sippach,[8] M. Sivertz,[3] H. D. Skank,[13] G. A. Sleege,[13] D. E. Smith,[29] G. Smith,[19] M. C. Smith,[29] A. Soldatov,[12] R. A. Soltz,[18] W. E. Sondheim,[19] S. Sorensen,[29,36] P. W. Stankus,[29] N. Starinsky,[21] P. Steinberg,[8] E. Stenlund,[20] A. Ster,[44] S. P. Stoll,[3] M. Sugioka,[31,37] T. Sugitate,[11] J. P. Sullivan,[19] Y. Sumi,[11] Z. Sun,[6] M. Suzuki,[39] E. M. Takagui,[33] A. Taketani,[31] M. Tamai,[41] K. H. Tanaka,[14] Y. Tanaka,[24] E. Taniguchi,[31,37] M. J. Tannenbaum,[3] V. Tarakanov,[30] O. Tarasenkova,[30] J. Thomas,[28] J. H. Thomas,[18] T. L. Thomas,[25] W. D. Thomas,[13] W. Tian,[6,36] J. Tojo,[17,31] H. Torii,[17,31] R.S. Towell,[19] V. Trofimov,[30] I. Tserruya,[42] H. Tsuruoka,[39] A. A. Tsvetkov,[16] S.K. Tuli,[4] H. Tydesjö,[20] N. Tyurin,[12] T. Ushiroda,[24] H. W. van Hecke,[19] A. A. Vasiliev,[16] C. Velissaris,[26] J. Velkovska,[28] M. Velkovsky,[28] W. Verhoeven,[22] A. A. Vinogradov,[16] M. A. Volkov,[16] A. Vorobyov,[30] E. Vznuzdaev,[30] J. W. Walker II,[29] H. Wang,[5] S. Wang,[9] Y. Watanabe,[31,32] S. N. White,[3] B. R. Whitus,[29] A.L. Wintenberg,[29] C. Witzig,[3] F.K. Wohn,[13] B.G. Wong-Swanson,[19] C.L. Woody,[3] W. Xie,[5,42] K. Yagi,[39] S. Yokkaichi,[31] G.R. Young,[29] I.E. Yushmanov,[16] W. A. Zajc,[8] Z. Zhang,[28] and S. Zhou[6]
(PHENIX Collaboration)

[1]Institute of Physics, Academia Sinica, Taipei 11529, Taiwan
[2]Bhabha Atomic Research Centre, Bombay 400 085, India
[3]Brookhaven National Laboratory, Upton, NY 11973-5000, USA
[4]Department of Physics, Banaras Hindu University, Varanasi 221005, India
[5]University of California - Riverside, Riverside, CA 92521, USA
[6]China Institute of Atomic Energy (CIAE), Beijing, People's Republic of China
[7]Center for Nuclear Study, Graduate School of Science, University of Tokyo, 7-3-1 Hongo, Bunkyo, Tokyo 113-0033, Japan
[8]Columbia University, New York, NY 10027 and Nevis Laboratories, Irvington, NY 10533, USA
[9]Florida State University, Tallahassee, FL 32306, USA
[10]Georgia State University, Atlanta, GA 30303, USA
[11]Hiroshima University, Kagamiyama, Higashi-Hiroshima 739-8526, Japan
[12]Institute for High Energy Physics (IHEP), Protvino, Russia
[13]Iowa State University, Ames, IA 50011, USA
[14]KEK, High Energy Accelerator Research Organization, Tsukuba-shi, Ibaraki-ken 305-0801, Japan
[15]Korea University, Seoul, 136-701, Korea
[16]Russian Research Center "Kurchatov Institute", Moscow, Russia
[17]Kyoto University, Kyoto 606, Japan
[18]Lawrence Livermore National Laboratory, Livermore, CA 94550, USA
[19]Los Alamos National Laboratory, Los Alamos, NM 87545, USA
[20]Department of Physics, Lund University, Box 118, SE-221 00 Lund, Sweden
[21]McGill University, Montreal, Quebec H3A 2T8, Canada
[22]Institut fuer Kernphysik, University of Muenster, D-48149 Muenster, Germany
[23]Myongji University, Yongin, Kyonggido 449-728, Korea
[24]Nagasaki Institute of Applied Science, Nagasaki-shi, Nagasaki 851-0193, Japan
[25]University of New Mexico, Albuquerque, NM, USA
[26]New Mexico State University, Las Cruces, NM 88003, USA
[27]Chemistry Department, State University of New York - Stony Brook, Stony Brook, NY 11794, USA
[28]Department of Physics and Astronomy, State University of New York - Stony Brook, Stony Brook, NY 11794, USA
[29]Oak Ridge National Laboratory, Oak Ridge, TN 37831, USA
[30]PNPI, Petersburg Nuclear Physics Institute, Gatchina, Russia

[31]RIKEN (The Institute of Physical and Chemical Research), Wako, Saitama 351-0198, JAPAN
[32]RIKEN BNL Research Center, Brookhaven National Laboratory, Upton, NY 11973-5000, USA
[33]Universidade de São Paulo, Instituto de Fisica, Caixa Postal 66318, São Paulo CEP05315-970, Brazil
[34]SUBATECH (Ecole des Mines de Nantes, IN2P3/CNRS, Universite de Nantes) BP 20722 - 44307, Nantes, France
[35]St. Petersburg State Technical University, St. Petersburg, Russia
[36]University of Tennessee, Knoxville, TN 37996, USA
[37]Department of Physics, Tokyo Institute of Technology, Tokyo, 152-8551, Japan
[38]University of Tokyo, Tokyo, Japan
[39]Institute of Physics, University of Tsukuba, Tsukuba, Ibaraki 305, Japan
[40]Vanderbilt University, Nashville, TN 37235, USA
[41]Waseda University, Advanced Research Institute for Science and Engineering, 17 Kikui-cho, Shinjuku-ku, Tokyo 162-0044, Japan
[42]Weizmann Institute, Rehovot 76100, Israel
[43]Yonsei University, IPAP, Seoul 120-749, Korea
[44]Individual Participant: KFKI Research Institute for Particle and Nuclear Physics (RMKI), Budapest, Hungary
[*]Deceased

Results from the PHENIX experiment for the first RHIC run with Au-Au collisions at $\sqrt{s_{NN}} = 130$ GeV are presented. The systematic variation with centrality of charged particle multiplicity, transverse energy, elliptic flow, identified particle spectra and yield ratios, and production of charged particles and π^0's at high transverse momenta are presented. Results on two-pion correlations and electron spectra are also provided, along with a discussion of plans for the second run at RHIC.

1. INTRODUCTION

The PHENIX experiment[1] has been designed to measure a broad variety of signals from both heavy ion and polarized proton-proton collisions at RHIC. The pursuit of penetrating probes generated in the early stages of the collision, combined with a program of hadron measurements, provides a detector with unparalleled capabilities to address observables sensitive to all stages of the collision process. This same detector is also very well-suited to the study of gluon and anti-quark contributions to the proton spin[2,3].

The PHENIX detector consists of three spectrometers: two muon spectrometers covering the full azimuth for $1.1 < |\eta| < 2.4$ and a central spectrometer consisting of two arms each subtending 90^o in azimuth and with $|\eta| < 0.35$. A central magnet provides an axial field, while each muon spectrometer contains a magnet that produces a roughly radial field. The central arms contain three tracking sub-systems: pad chambers (PC), drift chambers (DC) and time-expansion chambers (TEC); two forms of electromagnetic calorimetry (PbSc and PbGl); a time-of-flight hodoscope (TOF) and ring imaging Cerenkov counter (RICH). These sub-systems, together with a set of beam-beam counters (BBC) located in the region $3 < |\eta| < 3.9$, provide superb hadron and electron identification over a broad range of transverse momentum[4]. The muon spectrometers use cathode strip chambers in three stations for tracking (muTr), and five layers of Iarocci tubes interleaved with iron absorber for muon identification (muID). Global event characterization is achieved via a multiplicity and vertex detector (MVD) consisting of silicon strips and pads covering $|\eta| < 2.5$, and the RHIC-standard Zero-Degree Calorimeters (ZDCs), which detect neutral particles emitted along the beam directions[5,6]. The front end electronics for all sub-systems are clocked synchronously with the beam crossing frequency of 9.4 MHz. A set of Level-1 triggers derived from various sub-systems is used to initiate readout of the entire detector through a pipelined high bandwidth data acquisition system capable of archiving 20 MB/s.

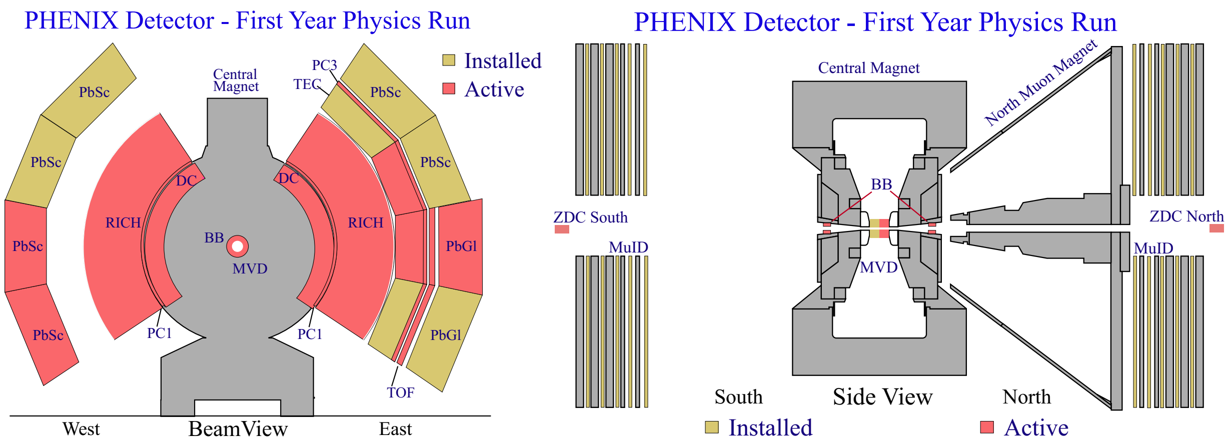

Figure 1. Installed and active detectors for the RHIC Run-1 configuration of the PHENIX experiment.

For the first physics run of RHIC in the summer of 2000, the portions of the PHENIX detector shown in Figure 1 were instrumented. Elements of all sub-systems, with the exception of the muTr, were in place and read out. Small subsets of the MVD and muID front end electronics were connected and tested as part of an engineering run. All other sub-systems were instrumented in fractions ranging from 25% to 100% of their ultimate aperture and were used in the physics results which are presented here. Independent minimum bias triggers were formed using coincidences between the BBC counters and between the ZDC counters. A total of approximately 5M events was recorded at $\sqrt{s_{NN}} =$ 130 GeV. The primary trigger used for most of the results presented below is based on the BBC coincidence with an additional offline requirement that restricts the collision vertex to $|z| < 20$ cm. Whenever possible, physics quantities are presented as a function of centrality and/or the number of participants N_{part}. Details on the determination of these quantities are presented in the following section and in the associated references.

2. GLOBAL OBSERVABLES

The systematic variation of particle yields and the produced transverse energy with the number of participants reflects the underlying reaction mechanisms. For example, Gyulassy and Wang[7] have emphasized that such a study can discriminate between cascade models and models which incorporate gluon saturation effects. PHENIX has studied the production near mid-rapidity of both charged particles and of transverse energy as a function of centrality. The deposition of energy in the ZDC's is correlated with that of charge in the BBC's to provide an unambiguous mapping between these observables and the centrality of the collision, as shown in Figure 2. A Glauber model is then used to

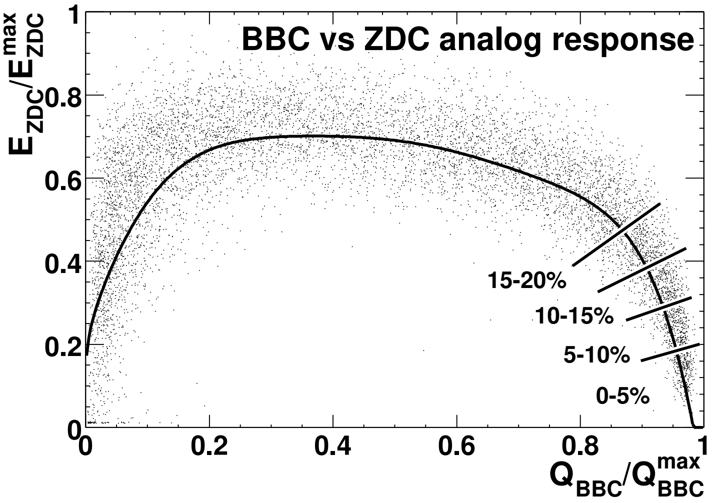

Figure 2. BBC vs ZDC analog response, related to the centrality classes of the collisions. The rightmost interval is the 0-5% centrality class, the next is 5-10% and so on.

determine the number of participants N_P and the number of binary collisions N_C for each centrality class. (This methodology is used consistently for all such studies presented in this contribution.)

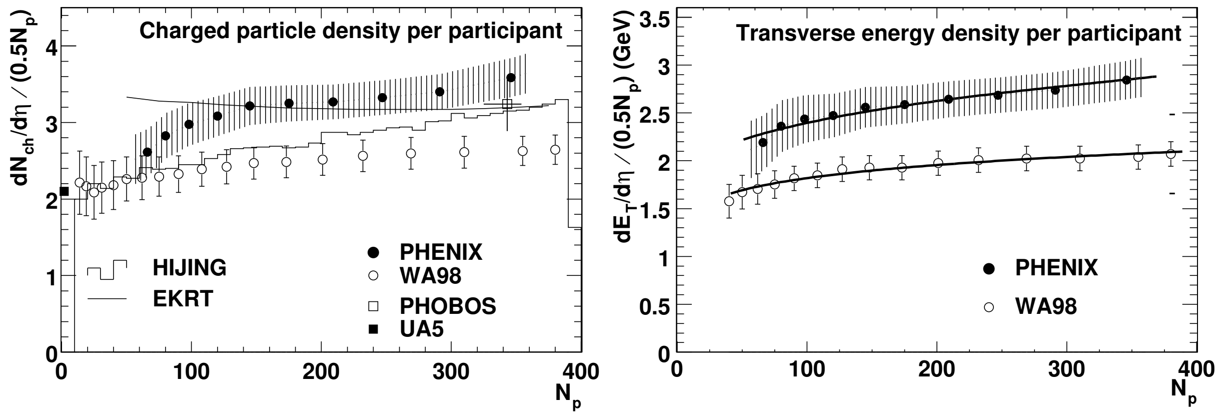

Figure 3. Left panel: The pseudorapidity density per participant pair versus the number of participants. Right panel: The transverse energy pseudorapidity density per participant pair versus the number of participants. The band in each figure indicates the systematic errors.

The number of produced charged particles is determined from the correlation between hits in two layers of Pad Chambers with the vertex location, which provides (on a statistical basis) the charged particle multiplicity distribution in the interval $|\eta| < 0.35$. After corrections for acceptance, efficiencies, decays and double hits, the charged particle pseudo-rapidity distribution $dN_{ch}/d\eta$ is calculated for each centrality bin, scaled by the corresponding number of participant pairs, then plotted versus N_P, as shown in Figure 3a. Also shown there are comparisons to the model predictions of EKRT[9,10], which does not reproduce the trend of the data. (Results very similar to the PHENIX data were reported at this conference by the PHOBOS Collaboration[11].)

A similar analysis has been performed for transverse energy measured in the PHENIX PbSc calorimeter[12]. A careful treatment of the contributions from produced energy in the aperture, the in-flux from scattering sources, and both the in-flux and out-flux from decays is performed to convert the deposited energy seen in the calorimeter to the equivalent transverse energy. The total transverse energy density per participant pair is then calculated in the same N_P bins as used in the multiplicity analysis. The trend, shown in Figure 3b., is essentially identical to that found for charged multiplicity, and indicates that particle and transverse energy production is not simply proportional to the number of participants. The yield may be described as a superposition of terms proportional to participants and binary collisions,

$$\text{Yield} = A \cdot N_P + B \cdot N_C \quad . \tag{1}$$

The results of this procedure are given in Table 1. The extent to which the ratio B/A is significantly different from zero may be taken as evidence for the role of binary collisions in contributing to production of particles and transverse energy at RHIC[13].

Table 1

Quantity	A	B	B/A
$dN_{ch}/d\eta$	0.88 ± 0.28	0.34 ∓ 0.12	0.38 ± 0.19
$dE_T/d\eta$	0.80 ± 0.24 GeV	0.23 ∓ 0.09 GeV	0.29 ± 0.18

The results of fits to Equation 1 for charged multiplicity and transverse energy near $\eta = 0$. Note the dimensions of A and B are different for the two analyses. The $\mp$ symbol in the error for B is used to indicate that its error is largely anti-correlated with that of A. This anti-correlation is propagated in calculating the error in the ratio B/A.

Also shown in Figure 3 are comparisons of both the charged multiplicity and the transverse energy per participant pair to the distributions measured by the WA98 collaboration at the CERN SPS[14], clearly demonstrating the increase of both quantities at RHIC. In the case of energy density calculated following the Bjorken prescription[15], the value of 4.6 GeV/fm^3 is roughly 60% larger[12] than that found at the SPS[16]. It is interesting to note that this increase does not result from an increase in $\langle dE_T/d\eta\rangle/\langle dN_{ch}/d\eta\rangle$; the value is very nearly equal to that found at the SPS[12].

Another global feature of hadronic production is the azimuthal pattern of emission, as parameterized by elliptic flow. Typically such analyses are performed with respect to the

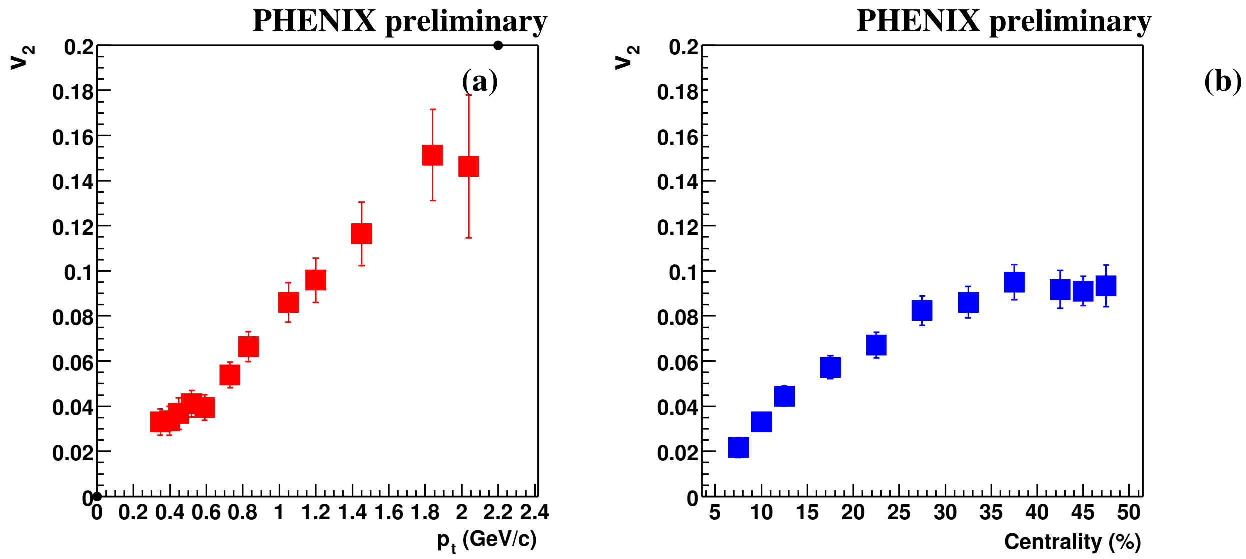

Figure 4. v_2 versus transverse momentum (a) and centrality (b). Errors are statistical only.

reaction plane determined for each event. It is also possible to determine the elliptic flow pattern by measuring the auto-correlation function of particles in the event, that is, by calculating the correlation function $C(\Delta\phi)$, where $\Delta\phi$ is the difference in azimuthal angle between two particles from the same event. PHENIX has performed such an analysis using charged particles with $p_T > 200$ MeV/c in the interval $|\eta| < 0.35$. The correlation function is calculated using an event-mixing prescription to determine the background distribution, then fit to extract the (assumed positive) v_2 coefficient:

$$C(\Delta\phi) \propto 1 + 2|v_1|^2 \cos(\Delta\phi) + 2|v_2|^2 \cos(2\Delta\phi) \tag{2}$$

Standard PHENIX event characterization methods are used to study the dependence of v_2 versus centrality in each p_T bin. A sample of the results[17] are shown in Figure 4. These trends, which are in good agreement with data from STAR[18] and preliminary results from PHOBOS[11], suggest that the high density matter formed at RHIC efficiently translates the initial spatial asymmetry into a corresponding one in momentum space.

3. IDENTIFIED HADRONS

The PHENIX central arm detectors have been designed to provide particle identification over the broadest possible momentum range[4]. The primary tool for charged hadron identification is the time-of-flight difference between the BBC and the highly-segmented TOF hodoscope, which spans $\Delta\phi = 45^o$ in the East spectrometer arm. The overall time resolution $\sigma \sim 115$ ps permits unambiguous π/K separation to at least $p_T = 1.5$ GeV/c. Normalized minimum bias p_T spectra for $\pi^{\pm}$, $K^{\pm}$, p's and $\bar{p}$'s are shown in Figure 5. The shape of the spectra clearly depends on the particle species, with pions having the lowest

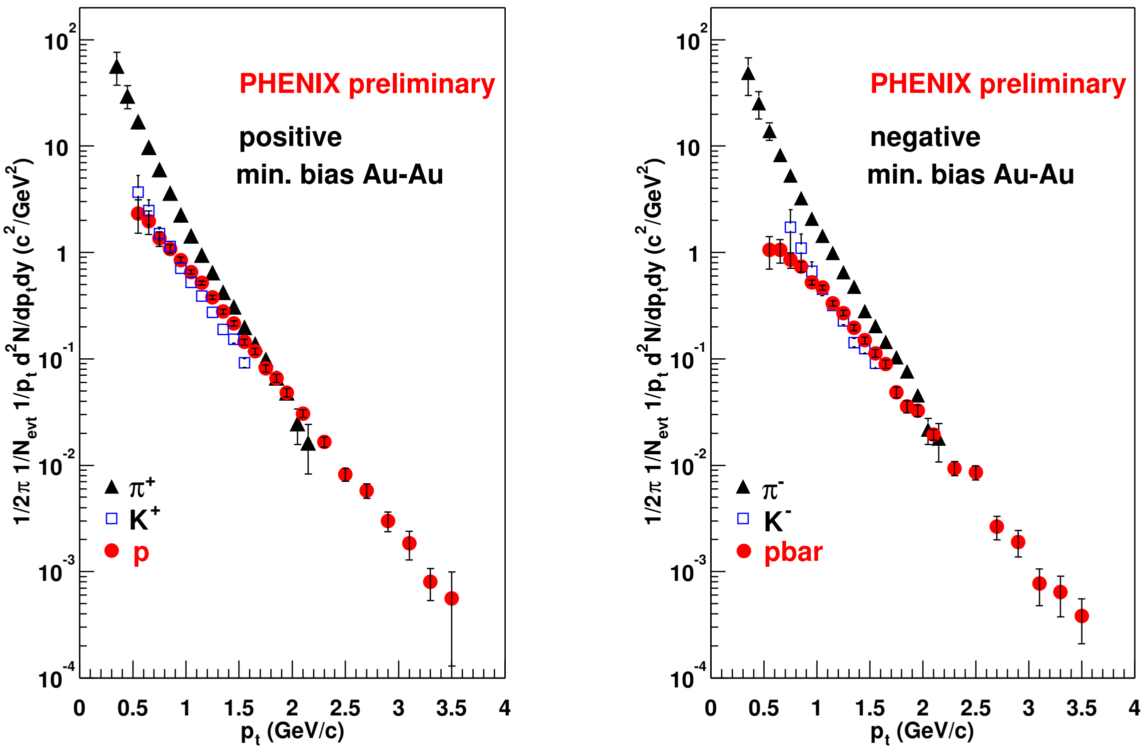

Figure 5. Normalized minimum bias transverse momentum spectra for positive (left) and negative (right) identified particles. The error bars are composed of statistical errors and the systematic errors associated with acceptance and decay corrections. There is an additional 20% systematic error associated with the overall normalization.

$\langle p_T \rangle$ and protons and anti-protons having the largest. The dependence of the local slopes increases with both centrality and with particle mass, consistent with expectations from radial flow[19].

The ratio of anti-protons to protons at $y = 0$ is of particular interest, since it is a direct measure of the net baryon content in the central region. The $\bar{p}/p$ ratio has been studied as a function of both transverse momentum and centrality[20], and found to be only weakly dependent on p_T and independent of centrality within systematic errors (Figure 6). For minimum bias collisions, the $\bar{p}/p$ ratio in the interval 0.8 GeV/c $< p_T <$ 3.0 GeV/c is 0.64 ± 0.01(stat.) $\pm\ 0.07$(sys.). This value (which is consistent with that observed by the other RHIC experiments[11,21,22]) together with the measured yields shown in Figure 5 signifies that the central region in heavy ion collisions at RHIC is meson-dominated, as distinct from the baryon-dominated case at the SPS and lower energies, where the ratio is never greater than ~ 0.1[23,24].

Charged pion pairs in the central arms have also been used to perform an HBT analysis. Two separate analyses were performed, one using pions identified with the TOF as described above, and the second in which the 700 ps time-of-flight resolution of the PbSc

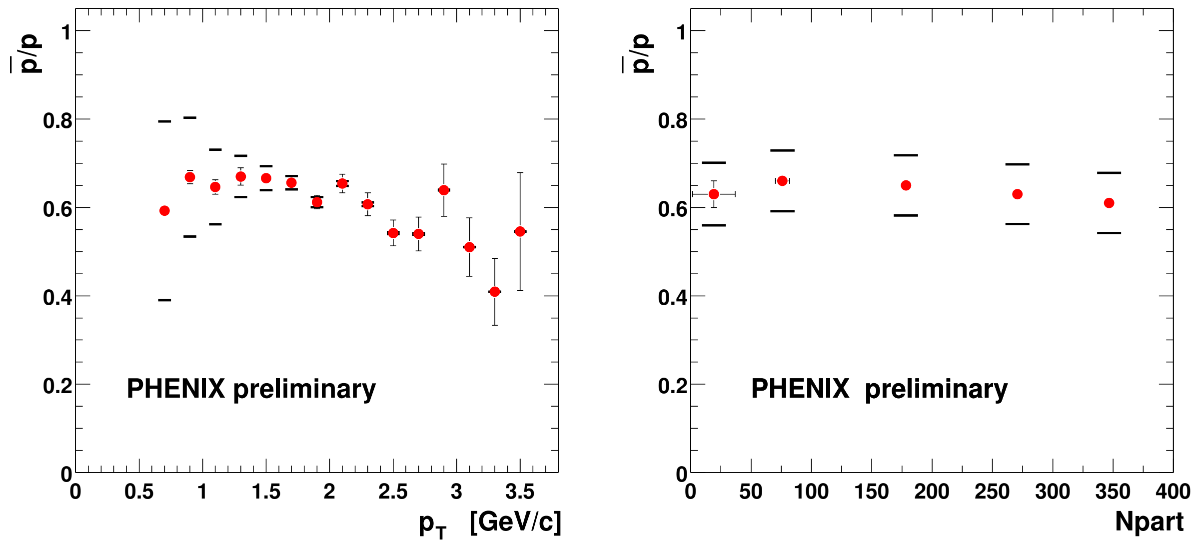

Figure 6. The $\bar{p}/p$ ratio versus transverse momentum for minimum bias Au-Au collisions (left) and versus centrality (right). For both figures, the error bars represent that statistical error on the ratio; systematic errors are indicated by the horizontal bars.

EmCal (EMC) is used to identify pions with transverse momentum $p_T < 0.7$ GeV/c. In addition to the obvious utility of comparing two independent data sets for this analysis, the larger acceptance of the EMC substantially increases the number of available pairs (by a factor of 5). Correlation functions are calculated in the standard $q_{Tside}, q_{TOut}, q_{Long}$ projections of the relative momentum for both $\pi^+\pi^+$ and $\pi^-\pi^-$ pairs and are then fit over the full 3D phase space to the form

$$C_2(q_{Tside}, q_{TOut}, q_{Long}) = 1 + \lambda \exp[-(q_{Tside}R_{Side})^2 - (q_{TOut}R_{Out})^2 - (q_{Long}R_{Long})^2] \quad . \quad (3)$$

The results, presented in Figure 7 and Table 2, show little if any variation from values obtained at lower energies. Given the significantly higher multiplicities and densities observed at RHIC, this is somewhat puzzling, and perhaps indicates significant dynamic effects on the radii from strong transverse expansion driven by these higher densities. In this context, it should be noted that the values of the radii and λ (for the TOF analysis), as well as the dependence on pair transverse momentum[25] are all consistent with measurements from the STAR collaboration[29].

4. PARTICLE PRODUCTION AT HIGH TRANSVERSE MOMENTUM

The high center-of-mass energy provided by RHIC, corresponding to values of $\sqrt{s_{NN}}$ where hard scattering at the partonic level is observed in p-p and p-$\bar{p}$ collisions, offers the exciting possibility of using perturbative probes amenable to quantitative calculation to explore hot nuclear matter. A first step in this program is the measurement of the transverse momentum spectrum for charged particles and its variation with the number of

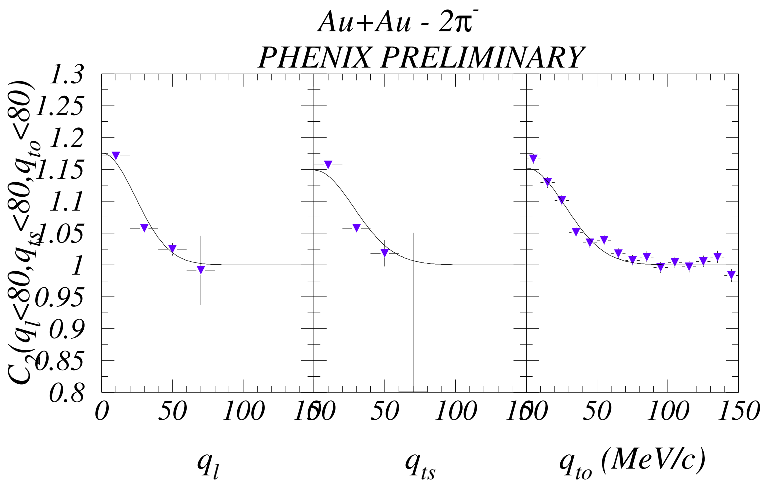

Figure 7. Correlation function for π^- pairs from the EMC analysis. The one-dimensional projections of the three-dimensional correlation function are averaged over the lowest 80 MeV/c in the other momentum differences. The fits are performed over the full phase space; the curves in the projections are averaged in the same manner as the data.

Table 2

Data Set	R_{Tout} (fm)	R_{Tside} (fm)	R_{Long} (fm)	λ
EMC $\pi^+\pi^+$	4.4 ± 0.2	5.1 ± 0.6	5.9 ± 0.4	$0.27 \pm .02$
TOF $\pi^+\pi^+$	6.2 ± 0.5	7.9 ± 1.1	4.0 ± 1.2	$0.49 \pm .05$
EMC $\pi^-\pi^-$	5.1 ± 0.2	5.0 ± 0.6	5.9 ± 0.4	$0.30 \pm .02$
TOF $\pi^-\pi^-$	5.5 ± 0.5	5.8 ± 1.5	6.7 ± 0.9	$0.49 \pm .06$

Results of the Bertsch-Pratt fits to the identical pion pairs in the EMC and TOF analyses. Only statistical errors are shown; current systematic uncertainties are < 1 fm.

participants in the collision. PHENIX has performed such an analysis using charged tracks reconstructed with the drift and pad chambers of the central arm[26]. The raw distribution of tracks is formed for six exclusive centrality classes, again using the standard PHENIX event classification described in Section 2. Corrections are made in each centrality bin for the spectral distortions due to momentum resolution and to backgrounds from scattering and decays. Results are shown in Figure 8 for the interval $0.4 < p_T < 5$ GeV/c, which spans six decades in yield.

In nucleon-nucleon collisions, production of high transverse momentum particles results from hard scattering at the partonic level. Since these cross sections are small, their contribution in nucleus-nucleus collisions, absent collective effects, should scale as the total number of binary collisions. For the most peripheral (80-92% in centrality) bin shown in Figure 8, the shape and yield above $p_T > 2$ GeV/c are in good agreement with an interpolation of hadron-hadron data[27] scaled by the number of binary collisions ($\langle N_{coll} \rangle = 3.7 \pm 2$) calculated for this centrality bin. This is not the case for the most central collisions, which show a deficit at large p_T with respect to N_{coll} scaling. This is

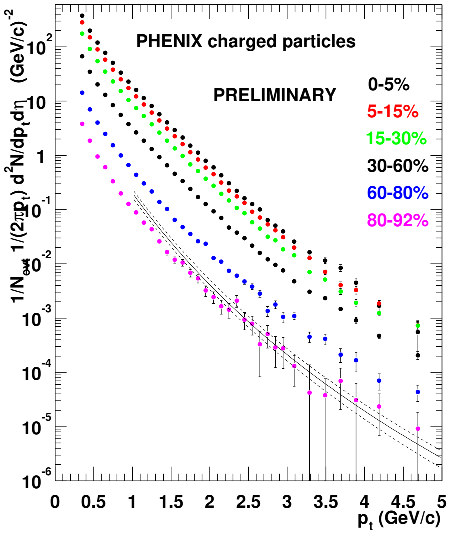

Figure 8. Normalized invariant transverse momentum spectra in the interval $|\eta| < 0.35$, for six centrality classes. The curve compares the most peripheral class (80-92%) to the yield expected from p-p collisions scaled by the corresponding number of binary collisions.

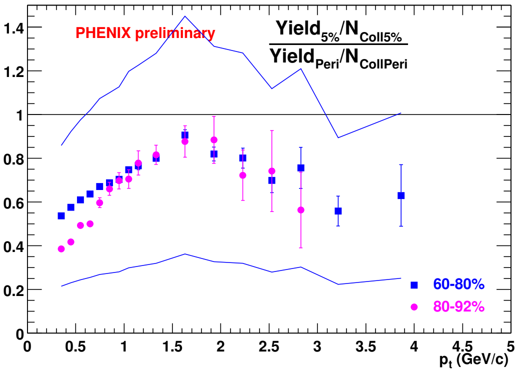

Figure 9. The p_T dependence of the ratio of yields for central (0-5%) collisions to yields for two peripheral classes (60-80% and 80-92%), scaled by the corresponding mean number of binary collisions for each centrality class.

presented in Figure 9, where the scaled ratio

$$\frac{Yield(Central)\ /\ \langle N_{coll}(Central)\rangle}{Yield(Peripheral)\ /\ \langle N_{coll}(Peripheral)\rangle} \tag{4}$$

is plotted for two different values of the peripheral reference set. The suppression at $p_T > 3$ GeV/c is inconsistent both with enhancements expected in that region for the Cronin effect[28] and also seen in PHENIX data for mid-peripheral data when scaled to the p-p reference distribution[26]. Similar results for such a suppression pattern in unidentified charged particles have been reported by the STAR collaboration[29].

An independent analysis by PHENIX provides further insight into the nature of the suppression[30]. The superb segmentation $\Delta\eta \times \Delta\phi = 0.01 \times 0.01$ and excellent resolution $8.2\%/\sqrt{E\ (\text{GeV})} \oplus 1.9\%$ of the PbSc electromagnetic calorimeter are used to extract the π^0 p_T spectrum by reconstruction (on a statistical basis) of their principal $\pi^0 \to \gamma\gamma$ decay mode. Extensive studies based on the mixing of single photon showers into both real and simulated events are used to determine the variation of the reconstruction efficiency with multiplicity and of the background with the event multiplicity. A detailed simulation is used to estimate the contributions from background and decay particles. Results are

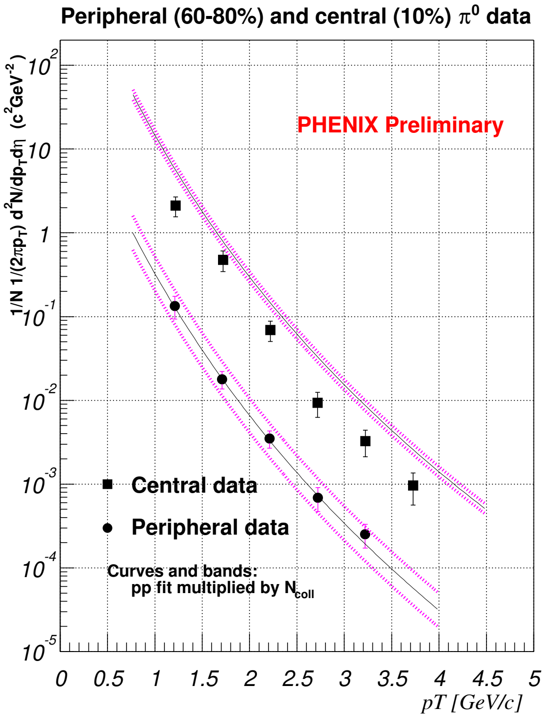

Figure 10. Normalized p_T spectra for π^0's from peripheral (60-80%) and central (0-10%) Au-Au collisions. The bands compare the data to the yield expected from p-p collisions scaled by the corresponding number of binary collisions; their width indicates the systematic uncertainty in the number of collisions used for scaling.

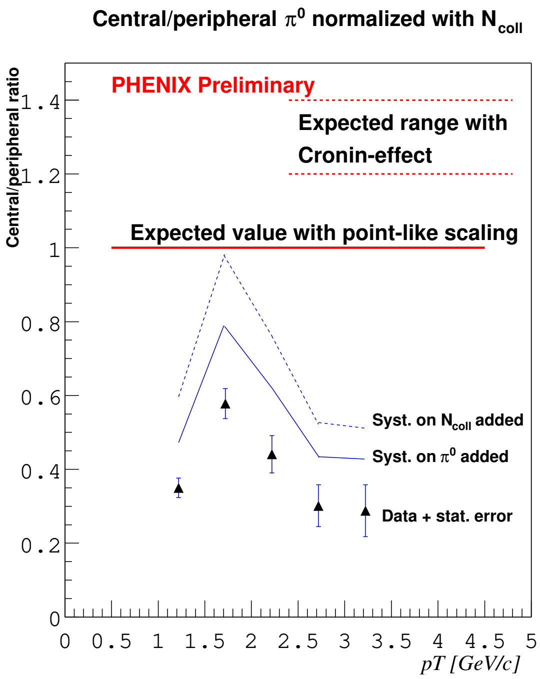

Figure 11. The p_T dependence of the ratio of π^0 yields for central (0-10%) collisions to yields for a peripheral collisions (60-80%), scaled by the corresponding mean number of binary collisions for each centrality class. The solid line represents the systematic error on the yields; the dashed line the additional systematic error from the uncertainty in the number of collisions used for scaling.

shown in Figure 10 for both a peripheral (60-80%) and central (0-10%) sample. As in the unidentified charged particle analysis, the peripheral data are well described with an interpolation of existing hadron-hadron data[27] scaled by the number of binary collisions. (An additional factor derived from p-p data of $\pi^0/(h^+ + h^-) = 1/3.2$ is used to scale the measured yield of unidentified charged particles to neutral pions.) Once again, the central data fall well below the corresponding yield expected if high p_T particle production scaled with the number of binary collisions. This is strikingly illustrated by the scaled ratio of Equation 4 for the central to peripheral yields, as shown in Figure 11.

A comparison of the ratio in Figure 9 for unidentified charged particles to that of Figure 11 for π^0's suggests that the suppression may be more pronounced in the case of identified (neutral) pions. Should this be established (the present understanding of the systematic errors does not permit a definite conclusion) a consistent description would imply that charged pions are also preferentially suppressed as compared to the unidentified charged particles. Hints of precisely this behavior are seen in Figure 5, where the trends in identified particle spectra suggest that the contributions from protons and anti-protons become comparable to those from pions for $p_T > 2$ GeV/c. Further work is required to improve both statistical and especially systematic errors to determine if the agreement of these data[30] with "jet quenching" predictions[31] is in fact evidence for an enhanced energy loss mechanism in hot nuclear matter. Clearly essential to that program is a set of detailed measurements of both p-p reference data and proton-nucleus collisions to determine the quantitative value of the Cronin effect at RHIC energies.

5. FUTURE PLANS

A major component of the PHENIX physics program is dedicated to measurement of leptonic signals. For example, the π^0 spectra described in Section 4, while intriguing and valuable in themselves, are also a prelude to the measurement of direct photons. In the central arms, virtual photons and vector mesons can be detected via their decays to e^+e^- pairs, while open charm and bottom production are expected to dominate the production of single electrons for p_T >2 GeV/c. Measurement of these signals requires π/e rejection in excess of 10^3 and very careful control of background contributions. Figure 12 shows the first efforts in this program[32]. Charged particles are tracked using the PHENIX drift and pad chambers. Electrons are selected by requiring that at least three PMT's fire in the RICH, and are further identified via a tight matching cut between tracking momentum and energy deposition in the EmCal.

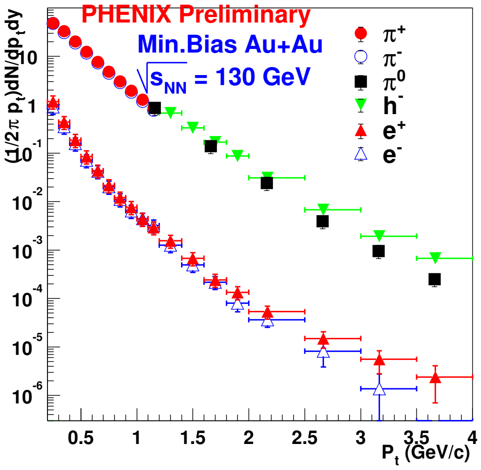

Figure 12. The inclusive spectrum of unidentified hadrons, $\pi^{\pm}$, π^0's and $e^{\pm}$ measured in Au-Au minimum bias collisions.

The power of this combined particle identification from the various PHENIX subsystems is apparent from Figure 12, where a clean electron spectrum is extracted at a level 2-3 orders of magnitude below that of all charged particles. This approach will form the basis for future PHENIX measurements of vector mesons and open charm at RHIC, and is also applicable to photon measurements via external conversion. The measurement of electrons along with all other PHENIX analyses will benefit greatly from the significantly enhancements made to the detector for Run-2 at RHIC. As shown in Figure 13, the complete aperture of the central arms will be available (compare to Figure 1), much of the MVD will be instrumented, and an entirely new spectrometer to measure muons will be

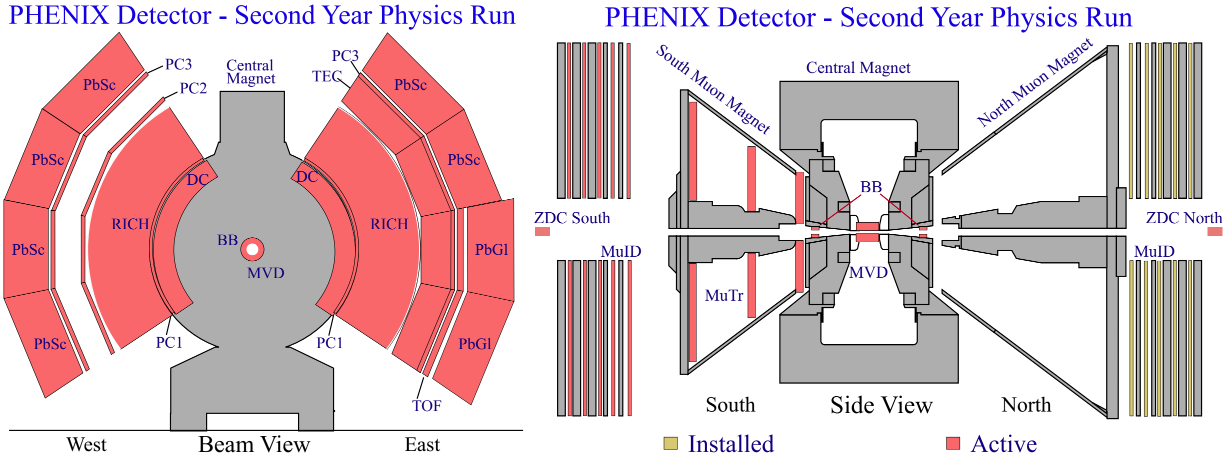

Figure 13. Installed and active detectors for the RHIC Run-2 configuration of the PHENIX experiment.

deployed. These additions in aperture and in capability, coupled with significant upgrades to the data acquisition and triggering system, should result in a hundredfold or more increase in the event sample obtained from Run-2. This will allow PHENIX to explore new signals and observables, to greatly increase statistical precision and understanding of systematic errors on existing analyses, to obtain the vital p-p comparison data, and to begin a program of measurements with polarized protons dedicated to understanding the proton spin.

6. ACKNOWLEDGMENTS

We thank the staff of the RHIC project, Collider-Accelerator, and Physics Departments at BNL and the staff of PHENIX participating institutions for their vital contributions. We gratefully acknowledge support from the Department of Energy and NSF (U.S.A.), Monbu-sho and STA (Japan), RAS, RMAE, and RMS (Russia), BMBF and DAAD (Germany), FRN, NFR, and the Wallenberg Foundation (Sweden), MIST and NSERC (Canada), CNPq and FAPESP (Brazil), IN2P3/CNRS (France), DAE (India), KRF and KOSEF (Korea), and the US-Israel Binational Science Foundation.

REFERENCES

1. D. P. Morrison *et al.* [PHENIX Collaboration], Nucl. Phys. A **638**, 565 (1998) [hep-ex/9804004].

   Current PHENIX information is available at http://www.phenix.bnl.gov/ .

2. N. Saito *et al.* [PHENIX Collaboration], Nucl. Phys. A **638**, 575 (1998) [hep-ex/9805003].

3. G. Bunce, N. Saito, J. Soffer and W. Vogelsang, Ann. Rev. Nucl. Part. Sci. **50**, 525 (2000) [hep-ph/0007218].
4. H. Hamagaki, for the PHENIX Collaboration, these proceedings.
5. S. White, for the PHENIX Collaboration, these proceedings.
6. C. Adler, A. Denisov, E. Garcia, M. Murray, H. Strobele and S. White, nucl-ex/0008005.
7. X. Wang and M. Gyulassy, Phys. Rev. Lett. **86**, 3496 (2001) [nucl-th/0008014].
8. K. Adcox *et al.* [PHENIX Collaboration], Phys. Rev. Lett. **86**, 3500 (2001) [nucl-ex/0012008].
9. K.J. Eskola, K. Kajantie and K. Tuominen, Phys. Lett. B **497**, 39 (2001) [hep-ph/0009246].
10. K.J. Eskola, K. Kajantie, P.V. Ruuskanen and K. Tuominen, Nucl. Phys. B **570**, 379 (2000) [hep-ph/9909456].
11. G. Roland, for the PHOBOS Collaboration, these proceedings, and references therein.
12. K. Adcox, Phys. Rev. Lett. **87**, 052301 (2001) [nucl-ex/0104015].
13. S. Milov, for the PHENIX Collaboration, these proceedings.
14. M.M. Aggarwal, *et al.*, [WA98 Collaboration], Eur. Phys J. **C18**, 651 (2001) [nucl-ex/0008004].
15. J.D. Bjorken, Phys. Rev. **D27**, 140 (1983).
16. NA49 Collaboration, T. Alber, *et al.*, Phys. Rev. Lett. **75**, 3814 (1995).
17. R. Lacey, for the PHENIX Collaboration, these proceedings.
18. K. H. Ackermann *et al.* [STAR Collaboration], Phys. Rev. Lett. **86**, 402 (2001) [nucl-ex/0009011].
19. J. Velkovska, for the PHENIX Collaboration, these proceedings.
20. H. Ohnishi, for the PHENIX Collaboration, these proceedings.
21. C. Adler *et al.* [STAR Collaboration], submitted to Phys. Rev.Lett. (2000).
22. I.G. Bearden *et al.* [BRAHMS Collaboration], submitted to Phys. Rev. Lett. (2001).
23. M. Kaneta et al. J. Phys.G: Nucl. Part. Phys. **23**, 1865 (1997).
24. H. Appelshäuser *et al.* [NA49 Collaboration], Phys. Rev. Lett. **82**, 2471 (1999) [nucl-ex/9810014].
25. S.C. Johnson, for the PHENIX Collaboration, these proceedings.
26. F. Messer, for the PHENIX Collaboration, these proceedings.
27. A. Drees, these proceedings.
28. J.W. Cronin *et al.*, Phys. Rev. **D11**, 3105 (1975).
29. J. Harris, for the STAR Collaboration, these proceedings, and references therein.
30. G. David, for the PHENIX Collaboration, these proceedings.
31. X.N. Wang, Phys. Rev. **C61**, 064910 (2000). [nucl-th/9812021].
32. Y. Akiba, for the PHENIX Collaboration, these proceedings.